

Dually emissive P,N-co-doped carbon dots for fluorescent and photoacoustic tissue imaging in living mice

Nargish Parvin^{1,3} · Tapas K. Mandal^{2,3}

Received: 28 November 2016 / Accepted: 26 January 2017 / Published online: 7 February 2017
© Springer-Verlag Wien 2017

Abstract Hydrothermal treatment of a mixture of ethylene diamine, phosphoric acid and citric acid under ambient pressure generates fluorescent carbon dots that are co-doped with phosphorus and nitrogen. These have features such as (a) both green fluorescence (peaking at 430 nm; 30% quantum yield) and red fluorescence (peaking at 500 nm, quantum yield 78%), (b) wavelength-dependent emission peaks, and (c) insensitivity to changes of pH values, dot concentration and ionic strength. The C-dots are useful for both fluorescent (FL) and photoacoustic (PA) imaging of living tissue. PA imaging warrants better spatial resolution and allows deeper tissues to be imaged compared to most optical imaging techniques. It is essential to assign a photoacoustic contrast agent as most of the diseases do not show a natural photoacoustic contrast in their early stage. The dually emitting C-dots are shown to be a useful contrast agent for PA and FL imaging of

mice tumors. Intravenous administration of the C-dots resulted in strong signals in both PA and FL imaging.

Keywords Carbon quantum dots · Dual emission · Quantum yield · Wavelength-dependent emission · Toxicity · Mouse tumor · Cancer diagnosis

Introduction

Excellent optical properties, high water solubility, surface modification flexibility, low toxicity, biocompatibility, photostability and easy synthesis make fluorescent carbon dots (CDs) attractive materials for use in chemical and biological sensing and bioimaging [1–4]. Synthetic approaches for CDs are mainly of the top-down or bottom-up approach [5, 6]. By the breaking down of large carbon source materials (like graphene sheet, graphite etc.) through arc discharge, laser ablation, chemical or electrochemical oxidation process used in top-down methods. Other C-dots are formed from molecular precursors under chemical reactions with different conditions in bottom-up methods. Due to the simplicity and the easy ability to produce different types of CDs, bottom-up method are preferred [7]. However, high emission quantum yields, low toxic, easy synthesis process of quantum dots are very rare and scientists are still struggling to develop the process. Normally carbon quantum dots emit blue color range under ultraviolet excitation [5, 7–9]. According to most of the reports the carbon dots absorb/emit in the visible region with a few exceptions [10]. The green, yellow and red fluorescence emission of CDs has been considered as a key requirement for the broad application in bioimaging but this tunability was achieved only rarely [8, 11, 12]. The emission of CDs are regulated by chemical surface

Both authors contributed equally to this work.

Electronic supplementary material The online version of this article (doi:10.1007/s00604-017-2108-4) contains supplementary material, which is available to authorized users.

- ✉ Nargish Parvin
Parvin@ipe.ac.cn; nargish.parvin@gmail.com
- ✉ Tapas K. Mandal
tpsmndl@iccas.ac.cn; tps.mndl@gmail.com

- ¹ Key Laboratory of Biochemical Engineering, Institute of Process Engineering, Chinese Academy of Sciences, No. 1, Bei Eijie, Zhongguancun, Beijing 100190, People's Republic of China
- ² Institute of Chemistry, Chinese Academy of Sciences, Bei Yi Jie 2, Zhongguancun, Beijing 100190, China
- ³ Department of Biotechnology, Indian Institute of Technology, Roorkee, Uttarakhand 247667, India

modifications and doping with other elements [6, 8]. Nitrogen is a very common doping element used along with boron, sulphur and phosphorus [13]. Excitation independent fluorescence emissions of CDs reported are very few where their emission is restricted blue to green only [1, 14]. So it is still difficult to synthesize a broad range of green to red fluorescence emissions CDs using a current strategy. However, the application of C-dots from the current synthesis methods is primarily subject to some limitations [10–12]. Till date focus has been on their fluorescent applications only [15], but their potential Photoacoustic (PA) imaging applications have not been widely explored yet. Fluorescence (FL) and photoacoustic (PA) molecular imaging techniques have different sensitivities, spatial resolutions, and imaging depths [16]. Due to the limited penetration depth fluorescence imaging technique is unsatisfactory in in-vivo applications. To overcome this inbuilt limitation of fluorescence imaging, multi-modal imaging probes like PA imaging or photothermal imaging are required to develop [17]. PA imaging has emerged as an innovative technique that enable imaging above the optical diffusion limit by integrating optical excitation with ultrasonic detection based on the PA effect, providing deeper tissue-imaging penetration and higher spatial resolution [18]. The combination of fluorescence and PA imaging into a single probe will be beneficial for tumor detection as it allows deeper tissue penetration while retaining imaging sensitivity compared to a single optical imaging methodology. PA imaging offers high-resolution structural images and fluorescence imaging provides high sensitivity to specific molecular probe for accurate true of tumor [19]. Instead of this various metal nanomaterials, dyes and fluorescence proteins have widely been employed as FL and PA imaging agents [20]. Thus current studies are ongoing in the search of low cytotoxic and rectified photostable nanomaterials for better imaging. Therefore, the development of an effective method to produce green and red dual emission P and N co-doped carbon quantum dots (PN-CQDs) as PA and fluorescence imaging agent for cancer diagnosis may reveal a new path for biomedical uses. Overall, these findings open up a new class of carbon quantum dots that are biocompatible and potentially can be employed in a wide range of biomedical applications.

Experimental

Chemicals and materials

All chemicals and materials used were purchased from Sigma-Aldrich (www.sigmaaldrich.com) and were used without further purification. Deionized water (Millipore Milli-Q

grade) with resistivity of 18.2 M Ω -cm was used in all experiments.

Physical characterization

The element binding environment of the samples was analyzed with an X-ray photoelectron spectroscopy (ESCALAB 250 spectrometer with a mono X-Ray source Al K α excitation (1486.6 eV). The spectra were corrected for background using the Shirley approach, and the surface composition of the samples was determined by measuring the ratio of C1s to N1 s, O1s or P2p intensities (integrated peak area) normalized by their respective sensitivity factors [1]. The morphology and microstructure of the synthesized sample PN-CQDs were characterized by a High-resolution transmission electron microscope (HRTEM) was carried out with JEM-2100F microscopes operating at 200 kV. The d-spacing of the sample was determined using Digital Micrograph software. Fluorescence spectroscopy was performed with a CARY Eclipse 5,5 fluorescence spectrophotometer and fluorescence spectra were measured using a 4 mL glass cuvette. UV-vis absorption spectra were obtained using a CARY 50 Conc UV-vis spectrophotometer. IR spectra were taken on a Nicolet Nexus Aligent 1100 series FT-IR spectrophotometer. The fluorescent images were taken at fluorescence microscopy (Carl Zeiss vert.A1 microscope, Carl Zeiss Micro imaging GmbH, 07740, Jena, Germany) using different band pass filtered 461 nm, 560 nm and 633 nm excitations and 5X, 10X, 20PX Objectives. The thermo gravimetric analysis (TGA) of the sample was performed on NETZSCH, TG 209 F3 Tarsus instrument in air from room temperature to 800 °C with a heating rate of 5 °C min⁻¹. It was calibrated with calcium oxalate.

Synthesis of phosphorous and nitrogen co-doped carbon quantum dots (PN-CQDs)

PN-CQDs were synthesized by hydrothermal treatment. Carbon source material citric acid (1.5 g) diluted in 10 mL of water and mixed well in stirrer, after addition of 10 mL H₃PO₄, amine source 1 mL ethylenediamine (EDA), and 0.01 mg EDC as a coupling agent the mixture was transferred into an 80 mL Teflon-lined stainless-steel autoclave and was heated at constant temperature of 250 °C for 2 h. After the reaction is over, the autoclave was cooled down naturally. Then, the resultant solution was centrifuged at 11200 x g for 10 min and collected materials redissolved in ethanol and again centrifuged. Typically, this purifying procedure was repeated for three cycles. And the resultant *PN-CQDs* solution was filtered through Millipore 0.22 μ m filter paper and then dispersed in water for further characterization and evaluation.

Cellular toxicity

Mouse leukemic monocyte macrophage cell line RAW 264.7 cells (1×10^4 cells/well) were cultured first for 24 h in an incubator (37 °C, 5% CO₂) and for another 24 h after the culture medium was replaced with 100 μL of Dulbecco's modified Eagle's medium (DMEM) containing the *PN-CQDs* at different doses (mg/mL). Then, 20 μL of 5 mg/mL MTT solution was added to every cell well. The cells were further incubated for 4 h, followed by removing the culture medium with MTT and then 100 μL of DMSO was added. The resulting mixture was shook for 10 min at room temperature. The optical density (OD) of the mixture was measured at 490 nm. The absorbance measured for an untreated cell population under the same experimental conditions was used as the reference point to establish 100% cell viability.

The cell viability was estimated according to the following equation:

$$\text{Cell Viability (\%)} = \left(\frac{\text{OD}_{\text{Treated}}}{\text{OD}_{\text{Control}}} \right) \times 100\%$$

(Where OD control was obtained in the absence of *PN-CQDs* and OD treated obtained in the presence of *PN-CQDs*).

Fluorescence imaging in vitro

The Mouse leukemic monocyte macrophage cell line RAW 264.7 cells were cultured in DMEM supplemented with 10% fetal bovine serum and 1% penicillin. 0.1 mg mL⁻¹ concentrated of *PN-CQDs* solution were prepared in DI water. After the well dispersion, an aliquot (typically 100ul) of the suspension was added to culture plate, then incubated at 37 °C in a 5% CO₂ incubator for 24 h. Prior to fixation of the cells on the slide for inspection with a fluorescence microscope, the excess *PN-CQDs* were removed by washing 3 times with phosphate buffer (Ph-7). The bioimaging was taken at Zeiss inverted fluorescent Microscope (Carl Zeiss vert.A1 microscope, Carl Zeiss Micro imaging GmbH, 07740, Jena, Germany).

Fluorescence/PA imaging in vivo

The fluorescence and PA images of a nude mouse bearing a subcutaneous tumor at the flank region of the right hind leg were acquired with a Maestro in vivo spectrum imaging system (Cambridge Research & Instrumentation, Woburn, MA). The tumor model used was established upon subcutaneous injection of SGC7901 cells ($\sim 5 \times 10^6$) into male BALB/c nude mice (4 to 6 weeks old) at the flank region of the right hind leg. Nude mice bearing SGC7901 tumor xenografts were anesthetized, and then the probe was intravenously injected

into the tumor (*PN-CQDs* (1 mg/mL, 100 μL) when the tumor size reached approximately 25 to 30 mm³. All animal experiments reported herein were performed according to a protocol approved by the Peking University Institutional Animal Care and Use Committee. The fluorescent scans were performed at various time points (0, 0.2, 1, 3, 6, and 24 h) post injection. The tumor-bearing mice were sacrificed by exsanguinations at 24 h post-injection, the tumor and major organs were harvested (heart, liver, spleen, kidneys, and Lung), cut into small pieces and then directly subjected to fluorescence/PA study. The excitation filter was a narrow-band filters to allow light with wavelength of 455, 523, 595, 605 nm to pass through; the emission filters was a 490, 560, 635 and 645 nm long-pass filter respectively. The exposure time for acquiring each fluorescence image was set at 300 ms. The Maestro optical system consists of an optical head that includes a liquid crystal tunable filter (with a bandwidth of 10 nm and a scanning wavelength range of 500 to 900 nm) with a custom-designed, spectrally optimized lens system that relays the image to a scientific-grade megapixel CCD. Prior to intravenous administration of the *PN-CQDs* (1 mg/mL, 100 μL), we first obtained pre-contrast data with excitation wavelength from 500 nm to 900 nm. Then, post-contrast data were acquired at various time points (0, 0.2, 1, 3, 6, and 24 h) after intravenous administration of *PN-CQDs* under the same scan wavelength ranges. The captured images can be analyzed by the vendor software, which uses spectral unmixing algorithms to separate auto fluorescence from chromophore signals.

Quantum yields (QY) measurements

Quinine sulphate (0.1 M H₂SO₄ as solvent; excited at 360 nm, QY = 0.54) and fluorescein (dissolved in 0.1 mol/l NaOH, excited at 440 nm, QY = 0.95) was chosen as standard. The QY of *PN-CQDs* (in water) was determined by slope method [2] by the reference of quinine sulphate and fluorescein: compared the integrated photoluminescence intensity and the absorbance value [several values (less than 0.1 at excitation wavelength) gave the curve] of the samples with that of the references.

Then used the equation: $\varphi_x = \varphi_{st}(K_x/K_{st})(\eta_x/\eta_{st})^2$.

Where φ is the QY, K is the slope determined by the curves and η is the refractive index. The subscript "st" refers to the standards and "x" refers to the unknown samples. For these aqueous solutions, $\eta_x/\eta_{st} = 1$.

Statistical analysis

All data presented in this study are the average \pm SE of the experiments repeated at least three times. Paired Student's *t*-test was performed.

Results and discussion

Encouraged by our findings, in this study, we prepared novel carbon quantum dots (PN-CQDs) by an easy, rapid and single step hydrothermal method of synthesis. The PN-CQDs shows dual wavelength emissions like green and red where quantum yields are 30% and 78% respectively. According to our best knowledge we are the first to report the P and N co-doped green and red dual fluorescence emission carbon quantum dots synthesis with high quantum yield red emission. The dual emission properties lay the foundation for the use of PN-CQDs in ratiometric sensing or other applications that can take advantage of a material with dual wavelengths emission properties [12].

Here 1.5 g citric acid diluted with 10 mL DI water solution, 10 mL *ortho*-phosphoric acid (for carbonization and phosphorous source), 1 mL ethylenediamine (EDA for nitrogen source) and 0.01 mg EDC as a coupling agent well mixture was heated in a teflon coated hydrothermal at 250 °C. Upon cooling in room temperature, the mixture become brownish. Then, the brownish solution was centrifuged at 11200 x g for 10 min and collected materials redissolved in ethanol and again centrifuged. Typically, this purifying procedure was repeated for three cycles. The palate following centrifugation contained the PN-CQDs which is highly soluble in DI water. The homogeneous solution is stable at room temperature for years. The transmission electron microscopy (TEM) image (see ESM Fig. S1a†) shows that the size and morphology of the prepared PN-CQDs is distributed in the range from 2 to 7 nm, with an average size of 4.5 nm (see ESM Fig. S1c†). The particles are near about spherical in structure. High-resolution TEM (HRTEM) images (see ESM Fig. S1b†) suggest that multiple types of particles are present and that single PN-CQDs may also possess domains of different structures. All particles showing crystallinity, with lattice spacing of 0.28 nm, 0.36 nm, and 0.56 nm, corresponding well to the spacing of the planes of carbon materials, respectively. Powder XRD spectra of the PN-CQDs confirmed the *d*-spacing obtained by HRTEM (see ESM Fig. S2†). Dynamic light scattering results shown in ESM Fig. S1d† reveal that the nanoparticles in DI water, phosphate buffer (pH -7) and serum (10%) exhibit a single scattering peak that slightly changed in serum but after the particle solution was stored at room temperature for 60 days that is unchanged. The excellent colloidal stability of the resultant PN-CQDs nanoparticles make them reliable for medical imaging application. The chemical environment of elements in the materials has been investigated by X-ray photoelectron spectroscopy (XPS) and the results (see ESM Fig. S3a†) indicate that the PN-CQDs are mainly composed of carbon, nitrogen, Phosphorus and oxygen i.e. suggestive of the incorporation of all reagents into the particles (see ESM Fig. S3a†). The high resolution spectrum of C1s exhibits five main peaks (see ESM Fig. S3b†). The binding

energy peak at 284.6 eV confirms the graphitic structure (sp² C-C) of the PN-CQDs. The peak at about 285.2 eV suggests the presence of C-N, the peak around 286.4 is assigned to C-P. Another two peaks are centered at ca 287.0 eV and 288.7 eV which denote C-O and O-C = O bonds respectively. The O 1s peaks were deconvoluted into four components (see ESM Fig. S3c†), corresponding to oxygen bonded to carbon (C - O)(531.3 eV) and non-bridging oxygen in the phosphate group (P = O)(532.0 eV), singly bonded oxygen (-O-) in C-O and in C-O-P groups (532.9 eV), chemisorbed oxygen (carboxylic oxygen, COO) and water (533.6 eV), and OH groups like in cyclohexanol or phenol (537.8 eV) [21]. The peak at 532.9 eV confirm that P-O possesses the largest amount of phosphorus groups.

The N 1s spectrum (see ESM Fig. S3d†) reveals the presence of tertiary amines of the type X₃-N (400.5 eV, X = C, N, or P), N-Q (Quaternary-N, 401.7 eV) and N-H (402.4 eV) groups, respectively [21]. The fine structure of P2p peak (see ESM Fig. S3e†) points to the presence of three major phosphorus groups differentiated by their binding energies: C3-P groups (133.0 eV); C-PO₃ and/or C2-PO₂ groups (134.5 eV); and C-O-P type groups (135.2 eV), such as (CO)₃PO, (CO)₂PO₂ and (CO)PO₃ [22–24]. Furthermore, in ESM Fig. S3f†, the Fourier transform infrared (FTIR) spectrum of PN-CQDs shows the characteristic peak at 536 cm⁻¹ emerges, which reflects the formation of vibration in plane of secondary amines -NH-; The appearance of 987 cm⁻¹ and 1162 cm⁻¹ assigned to vibration of P-O-C and P = O phosphate group, suggests the presence of phosphoric acid. The absorption band at 1417 and 1516 cm⁻¹ is related to the plane blending vibration and the stretching vibration of C-N, N-H from EDA. Other stretching are C-O (1658 cm⁻¹), C = O (1709 cm⁻¹), CH₂ (2984 cm⁻¹) and OH (3429 cm⁻¹) (see ESM Fig. S3f†). This FTIR result highly supports the XPS results. Moreover, the TGA analysis of the sample (see ESM Fig. S4†, Supporting Information) has shown that the sample is burned off completely after ca. 700 °C in air. The TGA results further confirm that highly surface modification of PN-CQDs. Thus, we hypothesize that *citric acid*, EDA, and H₃PO₄ condensed and partially carbonized under the strongly acidic, likely dehydrating, and oxidizing conditions (oxygen was not excluded during the synthesis), likely forming multiple chromophores type where EDC worked as coupling agent. Nitrogen is the most common dopant for fluorescent CDs [2, 3]. Co-doping a second heteroatom into N-doped carbon nanomaterials can modulate the electronic properties, tune the carbonaceous structure, polarizability and affect the catalytic activity [25]. Phosphorus-doping was introduced for the synthesis of almost all previously reported green fluorescent CDs [8, 9, 26]. Theoretical studies have predicted that defects induced by P doping or P,N co-doping can lead to the presence of a highly localized state close to the Fermi level [27]. Possibly co-doping of nitrogen and phosphorus affects the

degree of polymerization and graphitization. A higher graphitization degree induces a red-shift of fluorescence, resulting from the enhanced degree of π -conjugation and the decreased band gaps [28]. Other researchers proposed that formation of p–n type photochemical diodes through nitrogen and phosphorus co-doping into carbon dots increased quantum yield greatly [29]. We also believe that the co-doping of nitrogen and phosphorus into the PN-CQDs gives rise to their bright dual emission, but the exact structures and emission mechanisms of the PN-CQDs remain elusive. In ESM Fig. S5a†, the UV-vis absorption spectrum of a diluted sample of PN-CQDs in water exhibits a broad absorption band 200 to 800 nm (in inset of Fig. 3a visible to NIR region 400 to 800 nm) where one intense peak centred at 346 nm (Abs-1), attributed to π - π^* transitions of C = C, C = N, or N = P groups. Although at lower intensities, one more band centred at 450 nm (Abs-2) was also observed, indicative of extended conjugation (aromatic) structures [30]. These transitions centered about 340 nm and 450 nm due to the trapping of excited state energy by the surface states results in strong emission [31, 32]. The two maximum excitation wavelength 340 nm and 450 nm of the PN-CQDs are shown in ESM Fig. S5b, clearly demonstrating the presence of two major chromophores, with emission maxima at 430 and 500 nm respectively. The excitation wavelength-dependent emission spectra of the PN-CQDs at the excitation wavelengths from 340 to 570 nm are shown in ESM Fig. S5c. With an increase of the excitation wavelengths (340 to 370 nm), only one emission peak (centred at \sim 430 nm) is observed. Further increasing the excitation wavelengths (380, 390 nm) excites both emission; other hand excitation wavelengths (400–450 nm) only the emission peak (centred at about 500 nm) but after with the increasing of higher excitation (460 to 570 nm) the emission peak centre increasing. Above 580 nm, no fluorescence emission is recorded. The dual fluorescence emission of the PN-CQDs in the visible region of the spectrum is also clearly visible to the unaided eye (Fig. 1a). Different excitations wavelengths indicated elicited dual coloured emissions (green, and red). To our delight, the emitters are very bright, and the quantum yield of the two main emission bands are very high. The strongest red fluorescence emission centred at 500 nm ($\lambda_{\text{excitation}} = 450$ nm) possesses a high quantum yield of 0.78, while the other strongest green fluorescence emission band centred at 430 nm ($\lambda_{\text{excitation}} = 340$ nm) has a quantum yield of 0.30. Thus, the quantum yields of the PN-CQDs are higher than those of most previously reported CQDs and the highest for green and red CQDs emitters [5, 8, 9, 26, 33]. This is the best quantum yield performance according to the best of our knowledge (Table 1).

The halochromic responses of the emissions of the PN-CQDs at two wavelength in the range between pH 2 and 13 are shown in Fig. 1b and c. The PN-CQDs possess robust emissions that are only modulated to a minor degree (by about

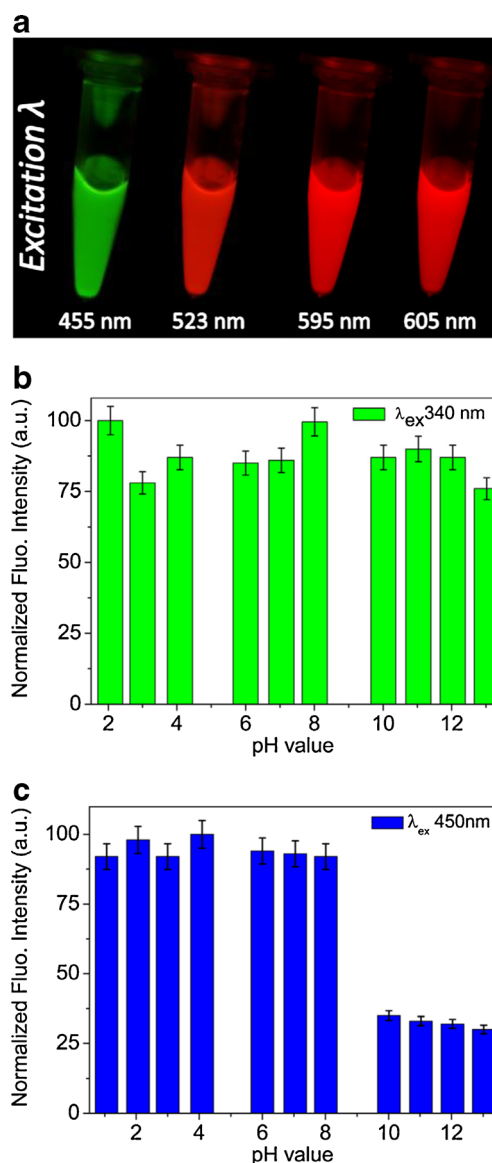


Fig. 1 a Photographs of PN-CQDs solutions (diluted in water), showing their excitation dependent emission properties. Excitation wavelengths indicated. Normalized fluorescent intensity of the PN-CQDs in the different pH range (b) fluorescent intensities at 430 nm ($\lambda_{\text{excitation}} = 340$ nm) and (c) at 500 nm ($\lambda_{\text{excitation}} = 450$ nm). The error bars represent standard error ($n = 3$)

23% and 50% at the extremes for excitation 340 nm and 450 nm respectively) by very high or low pH values. The absence of a very strong halochromic response is surprising in light of the fact that most previously reported CDs exhibit pH-dependent emission properties [1].

In case of the PN-CQDs it may indicate the absence of (many) amine-type nitrogens. On the other hand, the phosphoramidate-type nitrogens proposed to be present in the PN-CQDs are expected to be much less pH-sensitive, thus the pH-insensitivity provides another evidence for the presence of this functionality [12]. Furthermore the fluorescence stability

Table 1 Comparative performance chart of some carbon dots

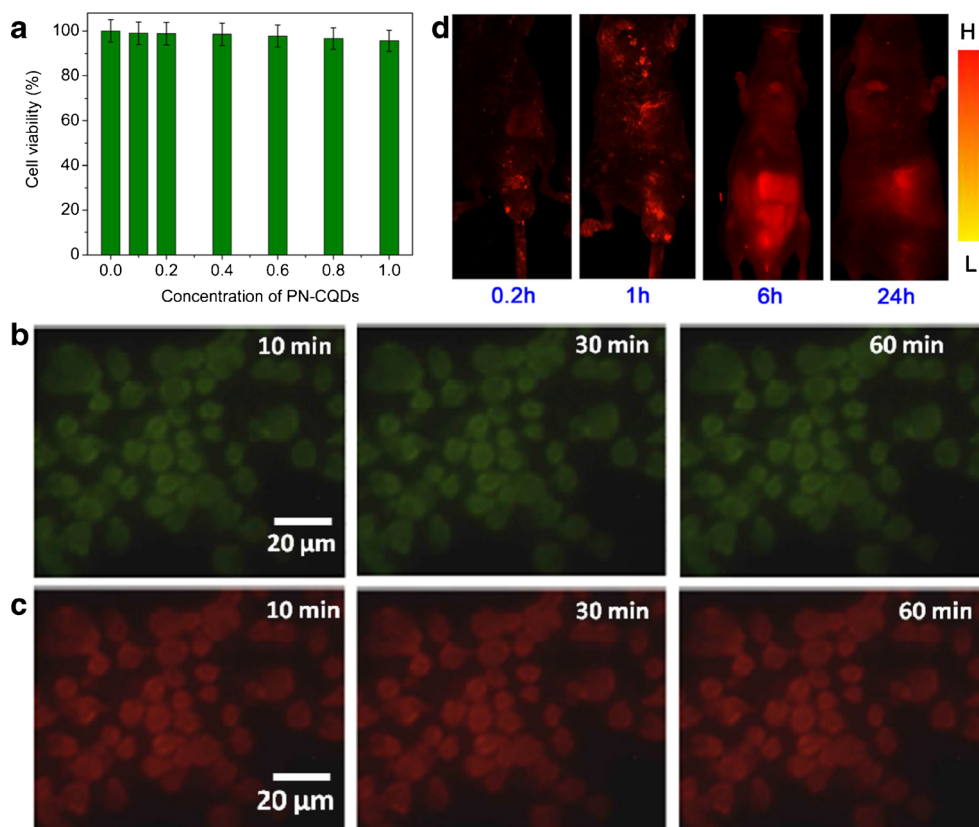
Material used	Applications	Exc/Em maxima	Quantum yield	References
Carbon dots	Cellular bioimaging	300/375 nm (single emissive)	11%	[34]
N,P doped carbon dots	Fluorescent cell imaging	340/418 nm (single emissive)	17.5%	[35]
Boron doped carbon dots	Determination of ferric ion	359/437 nm (single emissive)	Unknown	[36]
Carbon dots doped with nitrogen and sulphur	As a fluorescent probes and detection of biothiols	380/ 481 nm (single emissive)	10%	[37]
Carbon dots	Intracellular imaging of mercury(II)	340/440 nm, (single emissive)	13%	[38]
Carbon dots	As a fluorescent probes	360/451 nm (single emissive)	8–12%	[39]
N,P doped carbon dots	Fluorescence and photoacoustic tissue imaging	340/430 nm and 450/500 nm (dual emissive)	30–78%	This work

of PN-CQDs to the effects of the ionic strength was investigated. There was no change in fluorescence intensity or peak characteristics at different ionic strengths (see ESM Fig. S6†), which is significant because it is necessary for PN-CQDs to be used in the presence of physical salt concentrations in practical applications especially important for pharmaceutical applications. In order to investigate the biocompatibility of the synthesized PN-CQDs, a MTT assay was performed to assess the cytotoxicity of PN-CQDs by using mouse leukemic monocyte macrophage cell line RAW 264.7 and the results are shown in Fig. 2a. Cell viability was hardly affected when PN-CQDs concentration varied from 0 to 1 mg mL⁻¹ for 24 h. The cell survival rates still exceeded 97% at all the experimental

concentrations, indicating that the PN-CQDs have no apparent toxicity and are cyto-compatible with RAW 264.7 cells, which makes them a potential candidate for imaging in in-vivo. Here the RAW 264.7 cells were incubated with a PN-CQDs concentration of 1 mg mL⁻¹ and the imaging performance was examined to assess the cell viability by inverted fluorescence microscopy.

As shown in (Fig. 2b and c) all the RAW 264.7 cells exhibit the green and red-emissive where excitation 461 and 566 nm respectively. Under microscope no damage was observed in PN-CQDs treated cells without any photo bleaching for a long time period. The PN-CQDs are mainly incorporated into the cytoplasm region surrounding the

Fig. 2 In vitro FL imaging (a) relative viability of mouse leukemic monocyte macrophage cell line RAW 264.7 cells incubated with a series of gradient concentrations of PN-CQDs (0–1 mg mL⁻¹), The error bars represent standard error ($n = 5$). Real time in vitro fluorescence images of RAW 264.7 cells in different time period (b) green emission images and (c) red emission images, excitation at 460 nm and 562 nm respectively. d Real-time in vivo red fluorescence images after i.v. injection of PN-CQDs in nude mice at different time points



nucleus (Fig. 2b and c). All the above results reveal that PN-CQDs can be taken up by RAW 264.7 cells and serve

as a challenging bio-imaging agent. Figure 2d exhibits real-time in-vivo red fluorescence images after i.v. injection of

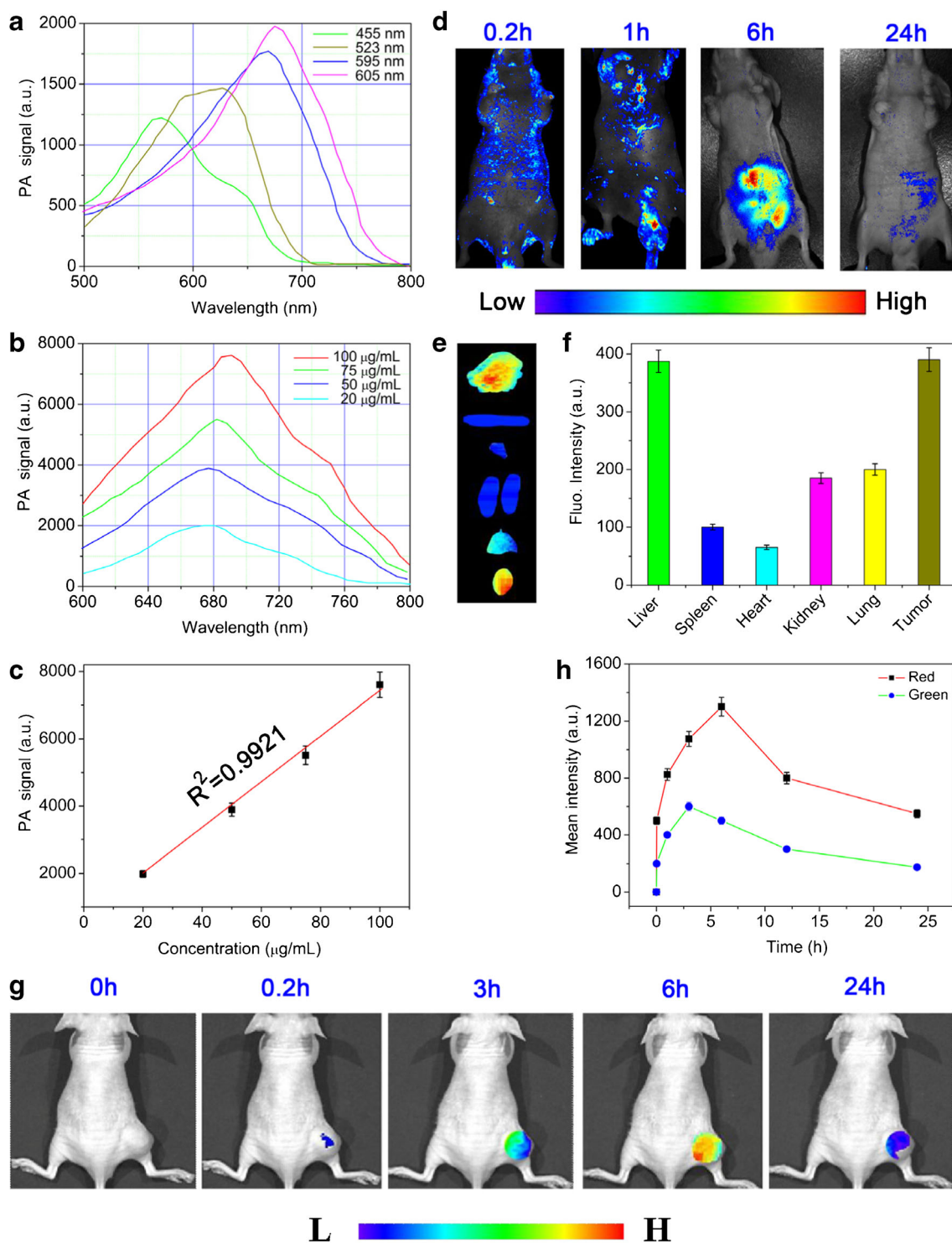


Fig. 3 Photoacoustic (PA) imaging **(a)** PA signals intensity range of 0.1 mg mL^{-1} PN-CQDs (in water under different excitation wavelength indicated). **(b)** PA signals of PN-CQDs with different concentrations. **(c)** Linear relationship between PA signal intensities and with different PN-CQDs concentrations. The error bars represent standard error ($n = 5$). **(d)** Real-time in vivo PA images after i.v. injection of PN-CQDs in nude mice at different time points. **(e)** Ex vivo images of mice tissues (from top to

bottom: heart, liver, spleen, lung, kidneys, and tumor). **(f)** Fluorescence intensity comparative graph of different harvested tissues. The error bars represent standard error ($n = 5$), **(g)** PA images of tumor (ROI-region of interest) in mice after i.v. injection with PN-CQDs at different time points. **(h)** Intensities of the mean signal and maximum mean signal of the ROI at different time points (0–24 h) after i.v. injection

C-dots in nude mice at different time points and ESM Fig. S7† represent the green and red emission in in-vivo imaging of tumor bearing nude mice. To denote the performance of PA imaging using the PN-CQDs, we studied the PA signal intensity spectrum of PN-CQDs under different excitation 455, 523, 595 and 605 nm where the emission spectrum of the PN-CQDs solution has a wide range in the visible to NIR region with red emission from 500 to 800 nm with a peak at 560, 640, 665 and 682 nm respectively (Fig. 3a). These results suggest that the PN-CQDs have stronger red emission character than green emission properties. In Fig. 3b the PA signals increased with the PN-CQDs concentration. Moreover, the PA signals were also observed to be linearly dependent on the concentration ($R^2 = 0.9921$) from 0 to 100 $\mu\text{g mL}^{-1}$ (Fig. 3c). Based on these results, we next examined the PN-CQDs for PA imaging in vivo. We studied the performance of PN-CQDs for in vivo PA imaging, in which tumor-bearing nude mice were selected as the animal model. Figure 3d shows the real time in-vivo PA images of mice intravenous (i.v.) injected with PN-CQDs (1 $\text{mg}\cdot\text{mL}^{-1}$, 100 μL). The nude mice not injected with PN-CQDs were selected as controls. After injection, the PN-CQDs spread all over the body organs as well as accumulated in the tumor area through the enhanced permeability and retention (EPR) effect (sometimes called passive targeting) [40].

The PA images of the tumors, which were recorded at various time points, predicted that PN-CQDs can extravagantly amassed in the tumor while preserving relatively constant PA signals after extended circulation in blood vessels during the whole imaging process. The dispersion of the long-circulating PN-CQDs in the tumor can render increased and distinct PA imaging of tumors in living mice. In supporting information Fig. S8 represent the significant deposition of PN-CQDs in tumor area. The mice were sacrificed at 24 h post-injection, major organs (heart, liver, spleen, lung, and kidneys) and tumors were removed and imaged to evaluate the fluorescence intensities within organs and tissues properly (Fig. 3e). The removed tumor and liver tissue showed strong fluorescence intensity, where the spleen and heart showed low signals (Fig. 3f). These in vivo results are similar with others previously reported C-dots [41, 11]. PN-CQDs deposition in the tumor as a region of interest (ROI) was further quantified by measuring its fluorescence intensity (Fig. 3g). The fluorescence signal in the tumor areas quickly increased within 0.2 h (12 min) post-injection due to the rapid deposition of PN-CQDs. The intensities of the mean signal of tumor increases with time after injection and reaches maxima at near about 3 h and 6 h post-injection for green and red emission respectively (Fig. 3h). This observation reveals a continuing deposition of PN-CQDs at the tumor area via blood circulation. So, the green and red-emissive PN-

CQDs will be used as a fluorescence imaging agent as well as NIR light-triggered PA imaging agent in vivo.

Conclusions

The synthesized nitrogen and phosphorus co-doped carbon quantum dots with high quantum yielding green (QY-30%) and red (QY-78%) dual emission. A highly reproducible, single-pot, rapid hydrothermal process was used to condense citric acid, phosphoric acid and EDA in aqueous solution. The PN-CQDs show only dual (green and red) fluorescence emission under different excitation wavelengths, with very high quantum yields, that are unaffected by changing pH values and strong ionic strength. Their high reproducibility of synthesis using competitive nano materials contributes itself to increase proportionally. The unique emission characteristics are assigned to the interactive effect of co-doping of nitrogen and phosphorus into the carbogenic material. The green and red-emissive PN-CQDs have the following characteristics: (1) broad absorption in the region from 400 to 800 nm, (2) active agents in PA and fluorescence imaging, (3) high pH and ionic tolerance strength and (4) visible light excitation (350–700 nm) for fluorescence and PA imaging in living mice. Based on the excellent photoluminescence properties, aqueous dispersibility, narrow size distribution, and low cytotoxicity, PN-CQDs can serve as promising probes for bioimaging applications. This study showed that the prepared PN-CQDs can be used as active agents in fluorescence and PA imaging, therefore importantly expanding the biomedical applications of C-dots like tumor detection and etc.

Acknowledgements TKM and NP would like to thank SERB, DST, (Project File no- SR/FT/LS-76/2012) and DBT Government of India for providing financial support respectively. Also thanks to “TWAS Programme” for financial support.

Compliance with ethical standards All animal experiments reported herein were performed according to a protocol approved by the Peking University Institutional Animal Care and Use Committee.

References

1. Krysmann MJ, Kellarakis A, Dallas P, Giannelis EP (2012) Formation mechanism of carbogenic nanoparticles with dual photoluminescence emission. *J Am Chem Soc* 134:747–750
2. Zhou J, Tang J, Deng S, Yan F, Li W, Qu M (2017) Carbon dots doped with heteroatoms for fluorescent bioimaging: a review. *Microchim Acta* 184:343. doi:10.1007/s00604-016-2043-9
3. Parvin N, Mandal TK, Roy P (2013) Polyelectrolyte carbon quantum-dots: new player as a noninvasive imaging probe in drosophila. *J Nanosci Nanotechnol* 13(10):6499–6505
4. Mandal TK, Parvin N (2011) Rapid detection of bacteria by carbon quantum dots. *J Biomed Nanotechnol* 7(6):846–848

5. Zhou J, Lin P, Ma J, Shan X, Feng H, Chen C, Chen J, Qian Z (2013) Facile synthesis of halogenated carbon quantum dots as an important intermediate for surface modification. *RSC Adv* 3: 9625–9628
6. Wolfbeis OS (2015) An overview of nanoparticles commonly used in fluorescent bioimaging. *Chem Soc Rev* 44(14):4743–4768
7. Zuo P, Lu X, Sun Z, Guo Y, He H (2016) A review on syntheses, properties, characterization and bioanalytical applications of fluorescent carbon dots. *Microchim Acta* 183:519–542. doi:10.1007/s00604-015-1705-3
8. Hu S, Trinchi A, Atkin P, Cole I (2015) Tunable photoluminescence across the entire visible Spectrum from carbon dots excited by white light. *Angew Chem Int Ed* 54:2970–2974
9. Shi Y, Pramanik A, Tchounwou C, Pedraza F, Crouch RA, Chavva SR, Vangara A, Sinha SS, Jones S, Sardar D, Hawker C, Ray PC (2015) Multifunctional biocompatible graphene oxide quantum dots decorated magnetic Nanoplatfrom for efficient capture and two-photon imaging of rare tumor cells. *ACS Appl Mater Interfaces* 7:10935–10943
10. Ge J, Lan M, Zhou B, Liu W, Guo L, Wang H, Jia Q, Niu G, Huang X, Zhou H, Meng X, Wang P, Lee CS, Zhang W, Han X (2014) A graphene quantum dot photodynamic therapy agent with high singlet oxygen generation. *Nat Commun* 5:4596. doi:10.1038/ncomms5596
11. Ge J, Jia Q, Liu W, Guo L, Liu Q, Lan M, Zhang H, Meng X, Wang PF (2015) Red-emissive carbon dots for fluorescent, photoacoustic, and thermal Theranostics in living mice. *Adv Mater* 27:4169–4177
12. Sun X, Brucknerb C, Lei Y (2015) One-pot and ultrafast synthesis of nitrogen and phosphorus co-doped carbon dots possessing bright dual wavelength fluorescence emission. *Nanoscale* 7:17278–17282
13. Parvin N, Mandal TK (2016) Synthesis of a highly fluorescence nitrogen-doped carbon quantum dots bioimaging probe and its in vivo clearance and printing applications. *RSC Adv* 6:18134
14. Jin SH, Kim DH, Jun GH, Hong SH, Jeon S (2013) Tuning the photoluminescence of graphene quantum dots through the charge transfer effect of functional groups. *ACS Nano* 7:1239–1245
15. Zhu A, Qu Q, Shao Z, Kong BT (2012) Carbon-dot-based dual-emission Nanohybrid produces a ratiometric fluorescent sensor for in vivo imaging of cellular copper ions. *Angew Chem Int Ed* 51:7185
16. Li C (2014) Imaging macrophages with nanoparticles. *Nat Mater* 13:110
17. Gaiduk A, Yorulmaz M, Ruijgrok PV, Orrit M (2010) Room-temperature detection of a single molecule's absorption by photothermal contrast. *Science* 330:353
18. Wang LV, Hu S (2012) Photoacoustic tomography: in vivo imaging from organelles to organs. *Science* 335:1458
19. Maeda A, Bu J, Chen J, Zheng G, DaCosta RS (2014) Dual in vivo photoacoustic and fluorescence imaging of HER2 expression in breast tumors for diagnosis, margin assessment, and surgical guidance. *Mol Imaging* 13:1
20. Pu K, Shuhendler AJ, Jokerst JV, Mei J, Gambhir SS, Bao Z, Rao J (2014) Semiconducting polymer nanoparticles as photoacoustic molecular imaging probes in living mice. *Nat Nanotechnol* 9:233
21. Nalwa HS (1991) Optical and X-ray photoelectron spectroscopic studies of electrically conducting benzimidazobenzophenanthroline type ladder polymers original research article. *Polymer* 32:802–807
22. Morgan WE, Stec WJ, Albridge RG, Wazer JRV (1971) π -bond feedback Interpreted from the binding energy of "2p" electrons of phosphorus. *Inorg Chem* 10:926–930
23. Wu XLR (2006) Inhibition of catalytic oxidation of carbon/carbon composites by phosphorus. *Carbon* 44:141
24. Rosas JM, Ruiz-Rosas R, Rodríguez-Mirasol J, Cordero T (2012) Kinetic study of the oxidation resistance of phosphorus-containing activated carbons. *Carbon* 50:1523
25. Zhang J, Zhao Z, Xia Z, Dai L (2015) A metal-free bifunctional electrocatalyst for oxygen reduction and oxygen evolution reactions. *Nat Nanotechnol* 10:444–452
26. Gong X, Hu Q, Paa MC, Zhang Y, Shuang S, Dong C, Choi MMF (2014) Red-green-blue fluorescent hollow carbon nanoparticles isolated from chromatographic fractions for cellular imaging. *Nanoscale* 6:8162–8170
27. Cruz-Silva E, Cullen DA, Gu L, Romo-Herrera JM, Muñoz-Sandoval E, López-Urías F, Sumpter BG, Meunier V, Charlier JC, Smith DJ, Terrones H, Terrones M (2008) Heterodoped nanotubes: theory, synthesis, and characterization of phosphorus-nitrogen doped multiwalled carbon nanotubes. *ACS Nano* 2:441–448
28. Gong X, Lu W, Liu Y, Li Z, Shuang S, Dong C, Choi MMF (2015) Low temperature synthesis of phosphorous and nitrogen co-doped yellow fluorescent carbon dots for sensing and bioimaging. *J Mater Chem B* 3:6813–6819
29. Ananthanarayanan A, Wang Y, Routh P, Sk MA, Than A, Lin M, Zhang J, Chen J, Sun H, Chen P (2015) Nitrogen and phosphorus co-doped graphene quantum dots: synthesis from adenosine triphosphate, optical properties, and cellular imaging. *Nanoscale* 7: 8159–8165
30. Amali AJ, Hoshino H, Wu C, Ando M, Xu Q (2014) From metal-organic framework to intrinsically fluorescent carbon nanodots. *Chem Eur J* 20:8279–8282
31. Wang X, Cao L, Yang ST, Lu F, Meziani MJ, Tian L, Sun KW, Bloodgood MA, Sun YP (2010) Bandgap-Like Strong Fluorescence in Functionalized Carbon Nanoparticles. *Angew. Chem.* 122: 5438–5442 *Angew Chem Int Ed* 49:5310–5314
32. Anilkumar P, Wang X, Cao L, Sahu S, Liu JH, Wang P, Korch K, Tackett KN II, Parenzan A, Sun YP (2011) Toward quantitatively fluorescent carbon-based "quantum" dots. *Nanoscale* 3: 2023–2027
33. Wang L, Zhu SZ, Wang HY, Qu SN, Zhang YL, Zhang JH, Chen QD, Xu HL, Han W, Yang B, Sun HB (2014) Common origin of green luminescence in carbon nanodots and graphene quantum dots. *ACS Nano* 8:2541–2547
34. Bhaire ML, Talib A, Khan MS, Pandey S, Wu HF (2015) Synthesis of fluorescent carbon dots via microwave carbonization of citric acid in presence of tetraoctylammonium ion, and their application to cellular bioimaging. *Microchim Acta* 182(13–14): 2173–2181
35. Li H, Shao FQ, Zou SY, Yang QJ, Huang H, Feng JJ, Wang AJ (2016) Microwave-assisted synthesis of N, P-doped carbon dots for fluorescent cell imaging. *Microchim Acta* 183(2):821–826
36. Wang F, Hao Q, Zhang Y, Xu Y, Lei W (2016) Fluorescence quenchometric method for determination of ferric ion using boron-doped carbon dots. *Microchim Acta* 183(1):273–279
37. Guo Y, Yang L, Li W, Wang X, Shang Y, Li B (2016) Carbon dots doped with nitrogen and sulfur and loaded with copper (II) as a "turn-on" fluorescent probe for cystein, glutathione and homocysteine. *Microchim Acta* 183(4):1409–1416
38. Yan F, Kong D, Luo Y, Ye Q, He J, Guo X, Chen L (2016) Carbon dots serve as an effective probe for the quantitative determination and for intracellular imaging of mercury (II). *Microchim Acta* 183(5):1611–1618
39. Simões EF, Leitão JM, da Silva JCE (2016) Carbon dots prepared from citric acid and urea as fluorescent probes for hypochlorite and peroxynitrite. *Microchim Acta* 183(5):1769–1777
40. Kobayashi H, Watanabe R, Choyke PL (2013) Improving conventional enhanced permeability and retention (EPR) effects; what is the appropriate target? *Theranostics* 4:81
41. Chong Y, Ma Y, Shen H, Tu X, Zhou X, Xu J, Dai J, Fan S, Zhang Z (2014) The in vitro and in vivo toxicity of graphene quantum dots. *Biomaterials* 35:5041